



1 **The paradox of assessing greenhouse gases from soils for nature-**
2 **based solutions**

3

4 **Authors:**

5 Rodrigo Vargas^{1*} and Van Huong Le¹

6

7 **Affiliations**

8 ¹Department of Plant and Soil Science, University of Delaware, Newark, DE, USA

9

10

11 *Corresponding Author

12 Rodrigo Vargas (rvargas@udel.edu)

13

14

15

16

17

18

19



20

21 **Abstract**

22 Quantifying the role of soils in nature-based solutions require accurate estimates of soil
23 greenhouse gas (GHG) fluxes. Technological advances allow to simultaneously measure
24 multiple GHGs and now is possible to provide complete GHG budgets from soils (i.e., CO₂,
25 CH₄ and N₂O fluxes). We propose that there is a conflict between the convenience of
26 simultaneously measuring multiple soil GHG fluxes at fixed time intervals (e.g., once, or
27 twice per month) and the intrinsic temporal variability and patterns of different GHG fluxes.
28 Information derived from fixed time intervals -as is commonly done during manual field
29 campaigns- had limitations to reproduce statistical properties, temporal dependence, annual
30 budgets, and associated uncertainty, when compared with information derived from
31 continuous measurements (i.e., automated hourly measurements) for all soil GHG fluxes. We
32 present a novel approach (i.e., temporal univariate Latin Hypercube sampling) that can be
33 applied to optimize monitoring efforts of GHG fluxes across time. We suggest that multiple
34 GHG fluxes should not be simultaneously measured at few fixed time intervals (especially
35 once a month), but an optimized sampling approach can be used to reduce bias and
36 uncertainty. These results have implications for assessing GHG fluxes from soils and
37 consequently reduce uncertainty on the role of soils in nature-based solutions.

38

39 **Keywords:** Carbon dioxide, methane, nitrous oxide, representativeness, uncertainty

40



41 **1. Introduction**

42 Soils are important for nature-based solutions for their role in climate mitigation potential
43 through the implementation of different natural pathways (Griscom et al., 2017; Bossio et al.,
44 2020). The climate mitigation potential of soils is dependent on multiple factors such as
45 weather variability (Kim et al., 2012), ecosystem type (Oertel et al., 2016), soil structure
46 (Ball, 2013), management practices (Shakoor et al., 2021), or disturbances (Vargas, 2012),
47 where soils can ultimately act as net sources or sinks of greenhouse gases (GHGs). Therefore,
48 accurate quantification of the magnitudes and patterns of soil GHGs fluxes is needed to
49 understand the potential of soils to mitigate or contribute to global warming across
50 ecosystems and different scenarios.

51 Most of our understanding of soil GHGs has come from manual measurements
52 performed throughout labor intensive field campaigns and experiments (Oertel et al., 2016).
53 While most studies around the world have focused on soil CO₂ fluxes (Jian et al., 2020),
54 there are early examples reporting coupled measurements of soil CO₂, CH₄ and N₂O fluxes
55 across tropical forests (Keller et al., 1986) and savannas (Hao et al., 1988), temperate forests
56 (Bowden et al., 1993) and peatlands (Freeman et al., 1993). These pioneer studies provided
57 an early view of the importance of integrated measurements of multiple soil GHG fluxes to
58 understand the net global warming potential of soils, but also demonstrate the technical
59 limitations and challenges associated with these efforts. For example, it is known that manual
60 measurements have the strength of providing good spatial coverage during field surveys but
61 provide limited information about temporal variability (Yao et al., 2009; Barba et al., 2021).

62 Technological advances have opened the opportunity to simultaneously measure
63 multiple soil GHG fluxes (i.e., CO₂, CH₄ and N₂O) at unprecedented temporal resolution
64 (e.g., hourly). These efforts have demonstrated differences in diel patterns and pulse events
65 (e.g., rewetting) due to wetting and drying cycles across tropical (Butterbach-Bahl et al.,



66 2004; Werner et al., 2007), subtropical (Rowlings et al., 2012), and temperate (Savage et al.,
67 2014; Petrakis et al., 2017) ecosystems. These approaches provide more accurate information
68 to calculate net GHG budgets and the global warming potential of soils (Capooci et al.,
69 2019). That said, performing automated measurements of multiple GHGs is expensive and
70 this approach usually has lower representation of the spatial heterogeneity within ecosystems
71 (Yao et al., 2009; Barba et al., 2021).

72 Ideally, we would like to measure everything, everywhere, and all the time, but this is
73 not possible due to logistical, technological, physical, and economic constraints. Light weight
74 and low powered laser-based spectrometers have reduced technical barriers for
75 simultaneously measuring multiple GHGs fluxes from soils, and it is now easier and faster to
76 perform discrete manual surveys across time. This opportunity creates a paradox concerning
77 when to measure different GHG fluxes from soils when performing manual measurements. In
78 general, researchers tend to perform simultaneous measurements of multiple GHGs during
79 manual surveys, but this convenience could result in biased information. We propose that
80 there is a conflict between the convenience of measuring multiple GHGs at few fixed time
81 intervals and the intrinsic temporal variability of magnitudes and patterns of different GHG
82 fluxes.

83 Here, we test how a subset of measurements derived from a fixed temporal
84 stratification (FTS) for simultaneous measurements (i.e., stratified sampling schedule) or
85 using an optimized sampling (i.e., temporal univariate Latin Hypercube sampling (*tuLHs*)),
86 compared with automated measurements of soil CO₂ ($F_A\text{CO}_2$), CH₄ ($F_A\text{CH}_4$), and N₂O
87 ($F_A\text{N}_2\text{O}$) fluxes in a temperate forest. We reveal that reporting measurements of GHG fluxes
88 using a FTS for simultaneous measurements, results in biased information of temporal
89 patterns and magnitudes. This study shows how a biased sampling schedule could influence
90 our understanding of GHG fluxes and ultimately the climate mitigation potential of soils.



91

92 **2. Materials and Methods**

93 *2.1 Study site*

94 The experiment was performed in a temperate forest located at the St Jones Estuarine
95 Reserve (a component of the Delaware National Estuarine Research Reserve [DNERR] in
96 Delaware, USA. The site has a mean annual temperature of 13.3 °C and mean annual
97 precipitation of 1119 mm. Soils are classified as Othello silt loam with a texture of 40% sand,
98 48% silt, and 12% clay within the first 10 cm (Petrakis et al., 2018). The dominant plant
99 species are bitternut hickory (*Carya cordiformis*), eastern red cedar (*Juniperus virginiana* L.),
100 American holly (*Ilex opaca*), sweet gum (*Liquidambar styraciflua* L.), and black gum (*Nyssa*
101 *sylvatica* (Marshall)). The site has a mean tree density of 678 stems ha⁻¹ and diameter at
102 breast height (DBH) of 25.7±13.9 cm (mean±SD) (Barba et al., 2021).

103

104 *2.2 Automated measurements of soil GHG fluxes*

105 We performed automated measurements (45 minutes time intervals) of soil emissions of three
106 GHGs (i.e., CO₂, CH₄ and N₂O) between September 2014–September 2015. Continuous
107 measurements of soil GHGs were taken by coupling a closed-path infrared gas analyzer (Li-
108 COR LI-8100 A, Lincoln, Nebraska) and nine dynamic soil chambers (Li-COR 8100–104)
109 controlled by a multiplexer (Li-COR 8100-104) with a cavity ring-down spectrometer
110 (Picarro G2508, Santa Clara, California). Detailed description of experimental design,
111 measurements protocol are described in previous studies (Petrakis et al., 2018; Barba et al.,
112 2021, 2019). Briefly, for each flux observation, we measured CO₂, CH₄ and N₂O
113 concentrations every second with the Picarro G2508 for 300 seconds and calculated fluxes (at
114 45 minutes time intervals) from the mole dry fraction of each gas (i.e., corrected for water
115 vapor dilution) using the SoilFluxPro software (v4.0; Li-COR, Lincoln, Nebraska, USA).



116 Fluxes were estimated using both linear and exponential fits and we kept the flux calculation
117 with the highest R^2 . We applied quality assurance and quality control protocols using
118 information from all three GHGs as established in previous studies (Petraakis et al., 2018;
119 Barba et al., 2021, 2019; Capocci et al., 2019; Petraakis et al., 2017). Using these time series,
120 we extracted values to represent discrete temporal measurements based on FTS and using an
121 optimization approach as described below.

122

123 *2.3 Temporal subsampling of time series*

124 Subsampling of time series was performed using FTS and a temporal optimization following
125 a univariate Latin Hypercube (*tuLHs*) approach. The difference between FTS and temporal
126 optimization is that the first approach is focused on a fixed schedule (e.g., sampling once per
127 month), and the second is focused on reproducing the statistical properties and temporal
128 dependence relationship of the original GHG time series with a subset of measurements. This
129 means that optimized subsamples may not be spaced systematically (e.g., every 15 days) and
130 selected dates may vary for each GHG flux due to their specific statistical properties and
131 temporal variability.

132 FTS represents a traditional schedule for performing manual measurements of GHG
133 fluxes from soils. The FTS is usually performed with manual measurements because they
134 require extensive logistical coordination due to travel time and costs, availability of
135 instrumentation (e.g., gas analyzers) and personnel to perform the measurements, and
136 weather conditions. During these scheduled visits researchers usually collect fluxes from all
137 three GHGs and analyze them in a systematic manner to calculate magnitudes and patterns
138 throughout the length of the experiment. Usually, researchers perform manual samples during
139 the early hours of the day (between 9 am and 12 pm) to avoid confounding effects due to
140 large changes in temperature and moisture as demonstrated by information summarized by



141 the soil respiration global database (Cueva et al., 2017; Jian et al., 2020). Consequently, we
142 selected subsamples from each original GHG time series (derived from automated
143 measurements) using flux measurements from 10 am at fixed intervals of once per month
144 (n=12), twice per month (n=24), or four times per month (n=48) starting on the first week of
145 available data from automated measurements.

146 We applied *tuLHs* as an alternative subsampling approach to obtain an optimized
147 subsample with the same univariate statistical properties and temporal dependence
148 relationship of the original GHG time series. Optimization was performed to select
149 subsamples for each GHG flux using the same number of samples as for fix temporal
150 stratification: twelve ($k=12$), twenty-four ($k=24$) or forty-eight ($k=48$) measurements
151 throughout the year of available data from automated measurements.

152

153 2.4 Temporal Univariate Latin Hypercube Sampling (*tuLHs*)

154 Let $S = \{(x_1, y_1, z_1), (x_2, y_2, z_2), \dots, (x_n, y_n, z_n)\}$ be observations of the variables X , Y and Z in a
155 time series, where X , Y and Z are soil GHGs (i.e., CO_2 , CH_4 and N_2O). Each variable of the
156 time series is characterized by two functions: the univariate probability distribution function
157 and the temporal dependency function. Once these two functions are known, then the behaviors
158 of the variable can be reproduced (Le et al., 2020; Chilès and Delfiner, 2009; Trangmar et al.,
159 1986; Pyrcz and Deutsch, 2014). The *tuLHs* consists of three steps: (1) modeling the univariate
160 behavior of the variable using the empirical cumulative univariate probability distribution
161 function; (2) modeling the temporal dependence using the empirical variogram function; and
162 (3) optimizing a subsample applying a global optimization method, differential evolution,
163 using the previously obtained variogram function as an objective function.

164 First, to model the univariate behavior of the variables from the observations of S , the
165 empirical univariate cumulative distribution function $F_n^*(x)$ of X is estimated by:



166
$$F_n^*(x) = \frac{1}{n} \sum_{i=1}^n I \{x_i \leq x\} \quad (1)$$

167 where I represents an indicator function equal to 1 when its argument is true, and 0 otherwise.

168 Similarly, the empirical univariate distribution function of the variables Y and Z can be derived.

169 Second, to model the temporal dependence of the variables from the observations of S , the

170 empirical temporal correlation function (i.e., temporal variogram function) $\gamma^*(t)$ of X is

171 estimated by:

172
$$\gamma^*(t) = \frac{1}{2N(t)} \sum_{i=1}^{N(t)} [X(t_i + t) - X(t_i)]^2 \quad (2)$$

173 where $N(t)$ is the number of pairs $X(t_i + t)$ and $X(t_i)$ are separated by a time t . The variogram

174 functions of the variables Y and Z are analogous. Third, To optimize the subsample it is

175 required to choose the “optimal” data points with the selected sample size (i.e., $k=12, 24$ or 48 ;

176 where $k \ll n$) that will have the same behavior of the original observations of S (i.e., GHG

177 fluxes derived from automated measurements). To achieve this objective we use the differential

178 evolution, a global optimization method (Storn and Price, 1997), using the variogram function

179 as an objective function. The procedure consists of dividing the univariate empirical probability

180 distribution in Eq. (1) into k equiprobable strata, which is equivalent to k ordered data subsets.

181 From each subset, only one value must be chosen to satisfy the condition of a univariate Latin

182 hypercube. The differential evolution method is applied to find the optimal points that

183 minimize the difference between the subsample variogram $\gamma(t)$ and the data variogram $\gamma^*(t)$

184 in Eq. (3).

185
$$OF_1 = \sum_{i=1}^{N(t)} [\gamma(t) - \gamma^*(t)]^2 \quad (3)$$

186 where OF is the objective function and the variograms $\gamma(t)$ and $\gamma^*(t)$ are calculated using Eq.

187 (2).



188

189 2.5 Statistical analyses

190 The t-test was used to compare the means and the Kolmogorov-Smirnov test to compare the
191 probability distribution of measurements derived from each different sampling protocol. All
192 tests were done with the 95% confidence level. In addition, their statistical properties such as
193 mean, median, standard deviation, first and third quartile are compared. The differences of
194 the experimental semivariograms were calculated as a comparison measure for the temporal
195 dependence of the samples and the original time series of GHG fluxes. For cumulative sums
196 of GHG flux, their mean is calculated as the most likely value and their quantile difference
197 between 97.5 and 2.5 is used to quantify the range of uncertainty.

198

199 3. Results

200 3.1 Relationships among GHG fluxes from soils

201 Justification in support of FTS for simultaneous measurements of GHG fluxes would require
202 evidence of strong linear correlations between magnitudes and temporal dependence among
203 soil GHG fluxes. First, we did not find strong linear relationships between any combination
204 of GHG fluxes from soils derived from automated measurements (Fig. A1). Therefore, our
205 data did not support the assumption that the magnitude of one GHG flux was associated with
206 a linear increase or decrease of another GHG flux. Second, semivariogram models
207 demonstrated differences in the temporal dependence for each GHG flux. Automated
208 measurements of soil CO₂ fluxes ($F_A\text{CO}_2$) showed a temporal dependence following a
209 Gaussian variogram model, with a nugget of 4, a sill plus nugget of 28, and a correlation
210 range of 80 days (Fig. A2a). Automated measurements of soil CH₄ fluxes ($F_A\text{CH}_4$) also
211 showed a temporal dependence but followed a spherical variogram model, with a nugget of
212 7×10^{-8} , a sill plus nugget of 1.5×10^{-7} , and a correlation range of 110 days (Fig. A2b). In



213 contrast, automated measurements of soil N₂O fluxes ($F_A\text{N}_2\text{O}$) did not show a temporal
214 dependence, where a pure nugget effect was present, and with a correlation range of 0 days
215 (Fig. A2c). Consequently, the magnitudes and temporal patterns of these GHG fluxes were
216 different and did not provide support in favor of FTS for simultaneous measurements.

217

218 3.2 Optimization of GHG sampling protocols

219 We applied a *tuLHs* approach to identify subsamples that had the same statistical properties
220 and temporal dependence for each one of the original GHG time series from automated
221 measurements. Subsamples were identified for twelve ($k=12$), twenty-four ($k=24$) or forty-
222 eight ($k=48$) measurements throughout the year for each GHG time series. All subsamples
223 represent measurements collected at 10 am. Our results show that the optimized measurement
224 dates were different for each GHG flux (Fig. 1), and we provide explicit examples for $k=24$
225 (Fig. 1) and $k=12, 48$ (Fig. A3, A4).

226 The optimized CO₂ subsamples were well distributed throughout the year for all
227 sampling scenarios (i.e., k from 12 to 48), because $F_A\text{CO}_2$ had a strong temporal dependence
228 and a small nugget effect with respect to the sill (Fig. A2a). The optimized CH₄ subsamples
229 were also relatively well distributed throughout the year, especially for scenarios of $k=24$ and
230 $k=48$, as $F_A\text{CH}_4$ also had a temporal dependence but with a higher nugget effect with respect
231 to the sill (Fig. A2b). Finally, the optimized N₂O subsamples were more difficult to define
232 especially with a small sample size (i.e., $k=12$; Fig. A3c) because $F_A\text{N}_2\text{O}$ did not have a
233 temporal dependence (Fig. A2c).

234

235 3.3 Differences in statistical properties and temporal dependency of subsamples

236 Overall, there were no statistically significant differences among the mean values derived from
237 automated measurements and those from FTS or the *tuLHs* approach (Fig. 2 for $k=24$; Fig. A5



238 for $k=12$; Fig. A6 for $k=48$; Tables A1 and A2). Although this appears to be a promising result,
239 the simple comparison of the means is not enough to fully evaluate the information derived
240 from different sampling scenarios. Here, we present results based on comparing the means,
241 standard deviation, probability distributions, and semivariograms derived from automated
242 measurements and the different sampling scenarios for all GHG fluxes.

243 The mean of $F_A\text{CO}_2$ was 5.9, while the mean for FTS 5.5 $\mu\text{mol CO}_2 \text{ m}^{-2} \text{ s}^{-1}$, and 5.9
244 $\mu\text{mol CO}_2 \text{ m}^{-2} \text{ s}^{-1}$ for the *tuLHs* approach with $k=24$ (Fig. 3a-c). These results were comparable
245 with the means derived from FTS (5.4 and 5.4 $\mu\text{mol CO}_2 \text{ m}^{-2} \text{ s}^{-1}$), and from the *tuLHs* approach
246 (6.2 and 5.9 $\mu\text{mol CO}_2 \text{ m}^{-2} \text{ s}^{-1}$) using $k=12$ and $k=48$, respectively (Figs. A5, A6; Table A1).
247 The standard deviation of $F_A\text{CO}_2$ was 3.9 and 3.2 $\mu\text{mol CO}_2 \text{ m}^{-2} \text{ s}^{-1}$ for FTS, and 3.9 $\mu\text{mol CO}_2$
248 $\text{m}^{-2} \text{ s}^{-1}$ for the *tuLHs* approach with $k=24$ (Figs. 3a-c). These results were comparable with the
249 standard deviations derived from FTS (3.1 and 3.3 $\mu\text{mol CO}_2 \text{ m}^{-2} \text{ s}^{-1}$), and from the *tuLHs*
250 approach (4.1 and 3.9 $\mu\text{mol CO}_2 \text{ m}^{-2} \text{ s}^{-1}$) using $k=12$ and $k=48$, respectively (Fig. A5, A6; Table
251 A1). Our results show that the semivariograms of optimized samples using the *tuLHs* approach
252 closely approximate the semivariograms of automated measurements for $k=24$ (Fig. 4a) and
253 $k=12$ and 48 (Figs. A7a, A8a). These results are consistent with the sums of absolute
254 differences between the semivariograms of the samples and the semivariogram of $F_A\text{CO}_2$ with
255 differences of 69.31, 54.39, 49.42 for FTS, and 5.69, 1.99, 1.39 for the *tuLHs* approach for
256 $k=12, 24, 48$, respectively (Table A2).

257 The mean of $F_A\text{CH}_4$ was -0.93, while -0.86 $\text{nmol CH}_4 \text{ m}^{-2} \text{ s}^{-1}$ for FTS and -0.94 nmol
258 $\text{CH}_4 \text{ m}^{-2} \text{ s}^{-1}$ for the *tuLHs* approach with $k=24$ (Fig. 3d-f). These results were also comparable
259 with the means derived from FTS (-0.83 and -0.88 $\text{nmol CH}_4 \text{ m}^{-2} \text{ s}^{-1}$), and from the *tuLHs*
260 approach (-0.87 and -0.92 $\text{nmol CH}_4 \text{ m}^{-2} \text{ s}^{-1}$) using $k=12$ and 48, respectively (Figs. A5, A6;
261 Table A1). The standard deviation of $F_A\text{CH}_4$ was 0.36 and 0.26 $\text{nmol CH}_4 \text{ m}^{-2} \text{ s}^{-1}$ for FTS, and
262 0.34 $\text{nmol CH}_4 \text{ m}^{-2} \text{ s}^{-1}$ for the *tuLHs* approach with $k=24$. These results were comparable with



263 the standard deviations derived from FTS (0.27 and 0.29 nmol CH₄ m⁻² s⁻¹), and from the *tuLHs*
264 approach (0.33 and 0.35 nmol CH₄ m⁻² s⁻¹) using $k=12$ and $k=48$, respectively (Figs. A5, A6;
265 Table A1). The semivariograms of optimized samples using the *tuLHs* approach closely
266 approximate the semivariogram of automated measurements for $k=24$ (Fig. 4b) and $k=12$ and
267 48 (Figs. A7b, A8b). Consequently, the sums of absolute differences between the
268 semivariograms of the samples and the semivariogram of $F_A\text{CH}_4$ were 0.63, 0.48, 0.49 for FTS,
269 and 0.06, 0.04, 0.02 for the *tuLHs* approach with $k=12, 24, 48$, respectively (Table A2).

270 Finally, the mean of $F_A\text{N}_2\text{O}$ was 0.45 and 0.61 nmol N₂O m⁻² s⁻¹ for FTS, and 0.51 nmol
271 N₂O m⁻² s⁻¹ for the *tuLHs* approach with $k=24$ (Fig. 3g-i). These results were also comparable
272 with the means derived from FTS (0.59 and 0.25 nmol N₂O m⁻² s⁻¹), and from the *tuLHs*
273 approach (0.58 and 0.49 nmol N₂O m⁻² s⁻¹) using $k=12$ and 48, respectively (Figs. A5, A6;
274 Table A1). The standard deviation of $F_A\text{N}_2\text{O}$ was 1.62 and 1.97 nmol N₂O m⁻² s⁻¹ for FTS, and
275 1.54 nmol N₂O m⁻² s⁻¹ for the *tuLHs* approach with $k=24$. These results were comparable with
276 the standard deviations derived from FTS (1.38 and 0.91 nmol N₂O m⁻² s⁻¹), and from the *tuLHs*
277 approach (1.58 and 1.54 nmol N₂O m⁻² s⁻¹) using $k=12$ and $k=48$, respectively (Figs. A5, A6;
278 Table A1). Our results show that there is no temporal dependence for N₂O fluxes, but the
279 semivariograms of optimized samples using the *tuLHs* approach closely approximate the
280 semivariogram of automated measurements for $k=24$ (Fig. 4c) and $k=12$ and 48 (Figs. A7c,
281 A8c). Consistently, the sum of absolute differences between the semivariograms of the
282 samples and the semivariogram of $F_A\text{N}_2\text{O}$ were 10.01, 12.25, 16.75 for FTS, and 0.82, 1.13,
283 3.57 for the *tuLHs* approach with $k=12, 24, 48$, respectively (Table A2).

284 These results show that the *tuLHs* approach reproduced with greater precision the
285 probability distribution and the temporal dependence of the time series derived from automated
286 measurements than FTS for all GHGs. In the next section, we explore the implications of these
287 differences for calculation of cumulative GHG fluxes.



288

289 3.4 Calculation of cumulative GHG fluxes

290 We calculated the cumulative flux for all GHGs using available information from automated
291 measurements (Fig. 2; Table A3). The cumulative sum for available measurements of $F_A\text{CO}_2$
292 was $5758.5 \text{ g CO}_2 \text{ m}^{-2}$ [893.9, 13860.8; 95% CI]; for $F_A\text{CH}_4$ was $-0.47 \text{ g CH}_4 \text{ m}^{-2}$ [-0.81, -
293 0.19; 95% CI]; and $0.63 \text{ g N}_2\text{O m}^{-2}$ [-0.75, 5.19; 95% CI] for $F_A\text{N}_2\text{O}$.

294 We used the mean for each GHG flux derived from the *tuLHs* approach or the FTS to
295 calculate the cumulative sum (Table A3). We found that the FTS underestimated the
296 cumulative flux (-8.4, -6.2, -7.1%) and the uncertainty (-32.6, -21.6, -19.3%) of $F_A\text{CO}_2$ for
297 $k=12, 24, 48$, respectively (Fig. 5a). In contrast, the *tuLHs* approach overestimated the
298 cumulative flux (6.5, 1.1, 0.1%) and underestimated the uncertainty (-9.1, -4.4, -3.7%) for
299 $k=12, 24, 48$, respectively (Fig. 5a).

300 The FTS underestimated the cumulative flux (-9.1, -6.1, -3.1%) and the uncertainty (-
301 31.8, -27.3, -15.9%) of $F_A\text{CH}_4$ for $k=12, 24, 48$, respectively (Fig. 5b). In contrast, the *tuLHs*
302 approach underestimated the cumulative flux (-6.1%) only for $k=12$, but underestimated the
303 uncertainty (-15.9, -6.8, -4.5%) for $k=12, 24, 48$, respectively (Fig. 5b).

304 The FTS substantially underestimated the cumulative flux (-168, -170, -173%) of
305 $F_A\text{N}_2\text{O}$ for $k=12, 24, 48$, respectively. Uncertainty was overestimated for $k=12$ and 24 (3.6
306 and 26%) and underestimated for $k=48$ (-31%; Fig. 5c). In contrast, the *tuLHs* approach
307 overestimated the cumulative flux (29.5, 13.4, 9.1%) for $k=12, 24, 48$, respectively (Fig. 5c).
308 This approach underestimated the uncertainty for $k=12$ and 24 by -11.2 and -13.8%, but
309 overestimated the uncertainty by 2.9% for $k=48$ (Fig. 5c). These results show that the *tuLHs*
310 approach consistently provided closer estimates for cumulative sums and uncertainty ranges
311 than a FTS for all GHG fluxes.

312



313 **4. Discussion**

314 Applied challenges, such as quantifying the role of soils in nature-based solutions, require
315 accurate estimates of GHG fluxes. To do this, two fundamental questions exist for designing
316 environmental monitoring protocols: where to measure and when to measure? Ultimately a
317 monitoring protocol aims to quantify the attributes of an ecosystem, so it can be compared in
318 time within that ecosystem or with other ecosystems. Because we cannot measure everything,
319 everywhere, and all the time, we can argue that any monitoring protocol has assumptions that
320 are based on physical, economic, social, and practical reasons to address a specific scientific
321 question. These assumptions for designing monitoring protocols could result in misleading,
322 biased or wrong conclusions and therefore is critical to assess the consequences of different
323 monitoring efforts. As Hutchinson described in “The Concept of Pattern in Ecology”, we do
324 not always know if a given pattern is extraordinary or a simple expression of something
325 which we may learn to expect all the time (Hutchinson, 1953).

326 Automated measurements of soil GHG fluxes have revolutionized our understanding
327 of the temporal patterns and magnitudes of these fluxes in soils (Vargas et al., 2011; Savage
328 et al., 2014; Bond-Lamberty et al., 2020; Tang et al., 2006). That said, these types of
329 measurements have limitations to represent spatial variability and have higher equipment
330 costs that limits their broad applicability across study sites (Vargas et al., 2011).
331 Consequently, discrete manual measurements are a common approach to simultaneously
332 measure multiple GHG fluxes and report patterns, budgets, and information to parameterize
333 empirical and process based models (Phillips et al., 2017; Wang and Chen, 2012). In this
334 study, we argue that the convenience of simultaneously measuring multiple GHGs using FTS
335 may result in bias estimates; therefore, optimization of sampling protocols is needed when
336 there is a limited number of measurements in time (i.e., $k=12, 24, 48$).



337 We show that the magnitude of one GHG flux is not associated with a linear increase
338 or decrease of another GHG flux, and the temporal dependencies of each GHG flux are
339 different from each other (Fig. A1). Therefore, it is not possible to infer the dynamics of one
340 GHG flux based solely on information from another under the assumption that they share
341 similar (or autocorrelated) biophysical drivers. Multiple studies have shown that the
342 importance of different biophysical drivers (e.g., temperature, moisture, light) is different for
343 soil CO₂, CH₄ or N₂O fluxes (Luo et al., 2013; Tang et al., 2006; Ojanen et al., 2010). Our
344 results show that soil CO₂ fluxes have a strong temporal dependence (Fig. A2a), likely as a
345 result of the strong relationship between these fluxes and soil temperature in temperate mesic
346 ecosystems (Hill et al., 2021; Bahn et al., 2010). The temporal dependence decreased for soil
347 CH₄ fluxes (Fig. A2b), where there is less evidence for such strong correlation with soil
348 temperature (Bowden et al., 1998; Castro et al., 1995), and where multiple variables are
349 usually needed to explain the variability of these fluxes (Luo et al., 2013; Castro et al., 1994).
350 Soil N₂O fluxes had no temporal dependence (Fig. A2c), showing a strong decoupling from
351 soil CO₂ and CH₄ fluxes (Wu et al., 2010), likely as a result of independent biophysical
352 drivers regulating soil N₂O fluxes (Luo et al., 2013; Bowden et al., 1993; Ullah and Moore,
353 2011).

354 To address the limitations of a FTS protocol, we propose a novel optimization
355 approach (i.e., *tuLHs*) to reproduce the probability distribution and the temporal dependence
356 of each original time series of GHG fluxes. Traditional approaches usually optimize
357 subsamples by either focusing on reproducing the probability distribution of the original
358 information (Huntington and Lyrintzis, 1998), or by focusing on reproducing the temporal
359 dependence of the original information (Gunawardana et al., 2011). The *tuLHs* is a simple
360 approach that consists of using the univariate probability distribution function and the
361 temporal correlation function (i.e., variogram) as objective functions for each GHG flux. Our



362 results show that optimized subsamples do not coincide in time for the three GHGs,
363 suggesting that information should be collected based on the specific statistical and temporal
364 characteristics of each GHG flux (Fig. 1). This study provides a proof of concept for the
365 application of the *tuLHs* and demonstrates how optimization can be performed to improve
366 estimates of soil GHG fluxes.

367 The more temporal data we can collect, the better, but in many cases measurement
368 protocols are limited to a few measurements per year (i.e., $k=12$ to 48). Our results
369 demonstrate that for a small sample size (i.e., $k=12$) the optimized measurements for soil CO₂
370 fluxes are consistently spread across the year, for soil CH₄ fluxes are centered within the
371 growing season, and for soil N₂O fluxes are concentrated within the fall season (Fig. 1a). Our
372 optimization approach shows how measurements can be distributed across time as more
373 samples are available (i.e., $k=24$ to 48; Fig. 1b-c) and demonstrates that optimization is
374 critical when a limited number of measurements are available. In other words, a few
375 measurements properly distributed across time provide better agreement with information
376 derived from automated measurements. We highlight that this optimization approach should
377 be tested across different ecosystems as it will result in site-specific recommendations. That
378 said, a similar conclusion was proposed for the spatial distribution of environmental
379 observatory networks, where a network of few sites properly distributed (e.g., across a
380 country) improves our understanding of the target variable than a spatially biased network
381 (Villarreal et al., 2019). Thus, the need for representativeness assessment of information
382 collected across time and space is needed for accurate evaluation of environmental
383 measurements and quantification of nature-based solutions.

384 An initial approach suggested no statistical differences among the mean flux values
385 derived from different sampling protocols. Arguably, this simplistic approach is a false-
386 negative due to biased information from the FTS that does not accurately represent the



387 probability distribution and the temporal variability of soil GHG fluxes (e.g., Figs. 3-4). In
388 contrast, the optimization approach resulted in closer probability distributions and temporal
389 variabilities for all GHGs, providing additional evidence against the FTS approach.

390 There are several implications of biased monitoring protocols for the understanding of
391 soil GHG fluxes and nature-based solutions. First, temporal patterns and temporal
392 dependency may not be properly represented with the FTS approach. Soil GHG fluxes have
393 complex temporal dynamics that vary from diurnal to seasonal and annual scales that FTS is
394 not able to reproduce (Barba et al., 2019; Bréchet et al., 2021). Second, soil GHG fluxes
395 could present hot-moments, which are transient events with disproportionately high values
396 that are often missed with a FTS approach (Vargas et al., 2018; Butterbach-Bahl et al., 2004).
397 Third, cumulative sums and uncertainty ranges are biased or misleading when derived using a
398 FTS approach (Capooci and Vargas, 2022; Tallec et al., 2019; Lucas-Moffat et al., 2018). For
399 this third point, our study demonstrates that an optimized approach consistently provided
400 closer estimates for cumulative sums and uncertainty ranges when compared with automated
401 measurements (Fig. 5). We postulate that representing the variability of soil N₂O fluxes is
402 more sensitive to the FTS approach (>170% and >30% for cumulative sums and uncertainty
403 ranges, respectively) than for soil CH₄ and CO₂ fluxes. Fourth, it is possible that if
404 information derived from the FTS approach is biased, then functional relationships could also
405 be different from those derived from automated measurements (Capooci and Vargas, 2022).
406 It has been discussed that hypothesis testing and our capability for forecasting responses of
407 soil GHG fluxes to changing climate conditions is also biased with information from the FTS
408 approach (Vicca et al., 2014). Finally, because soils have a central role for nature-based
409 solutions within countries and across the world (Griscom et al., 2017; Bossio et al., 2020),
410 accurate measurements are required to properly assess management practices, environmental
411 variability and the contribution of GHGs from soils (Anderegg, 2021).



412

413 **Conclusion**

414 We highlight that we do not always know if a given pattern is extraordinary or a simple
415 expression of something which we may learn to expect all the time (Hutchinson, 1953).
416 Furthermore, the “Knowledge Paradox” has been recognized for soil science, where
417 innovative knowledge has often not been accepted by or implemented in society (Bouma,
418 2010). Here, we postulate that with emergent technologies there is a convenience of
419 measuring multiple GHGs from soils; however, few measurements collected at fixed time
420 intervals results in biased estimates.

421 We recognize that potential bias in measurements is dependent on the magnitudes and
422 temporal patterns of each GHG flux and could be site-specific. Nevertheless, evaluations are
423 needed to quantify potential bias in estimates of GHG budgets and information used for
424 model parameterization and environmental assessments. In this study, we propose a novel
425 optimization approach (i.e., temporal univariate Latin Hypercube sampling) that can be
426 applied with site-specific information of different ecosystems to improve monitoring efforts
427 and reduce bias of GHG flux measurements across time. We highlight that constant biased
428 environmental monitoring may provide confirmatory information which we have learned to
429 expect, but modifications of monitoring protocols could shed light into extraordinary
430 patterns. These unexpected patterns are the ones that will test paradigms and push science
431 frontiers.

432

433 *Data Availability.* All data used for this analysis is available at:

434 <https://doi.org/10.6084/m9.figshare.19536004.v1>

435



436 *Author Contributions.* R.V. conceived this study and V.H.L. designed and performed the
437 primary analysis with input from R.V in all phases. R.V. wrote the manuscript with input
438 from V.H.L.

439

440 *Competing Interest Statement.* None

441

442 *Acknowledgments.* The authors thank the Delaware National Estuarine Research Reserve
443 (DNERR), the personnel from the St Jones Reserve for their support throughout this study.

444 Authors acknowledge the land on which they realized this study as the traditional home of
445 the Lenni-Lenape tribal nation (Delaware nation). This study was funded by a grant from the
446 National Science Foundation (#1652594).

447

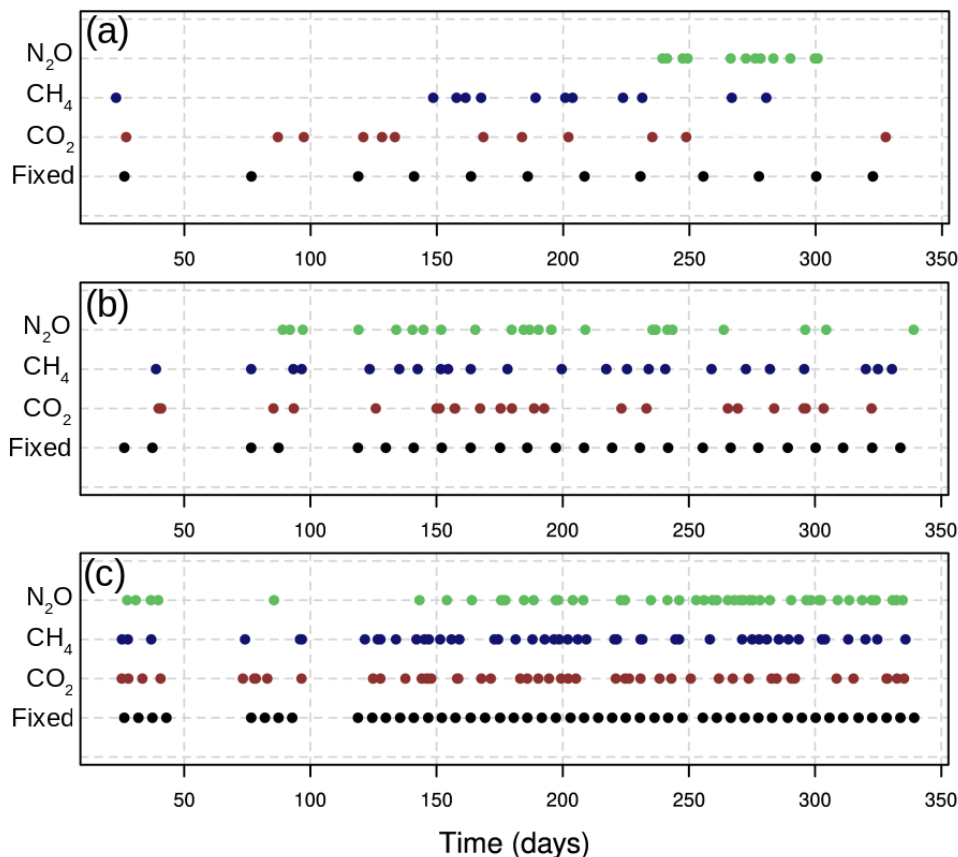
448

449

450



451 FIGURES
452
453

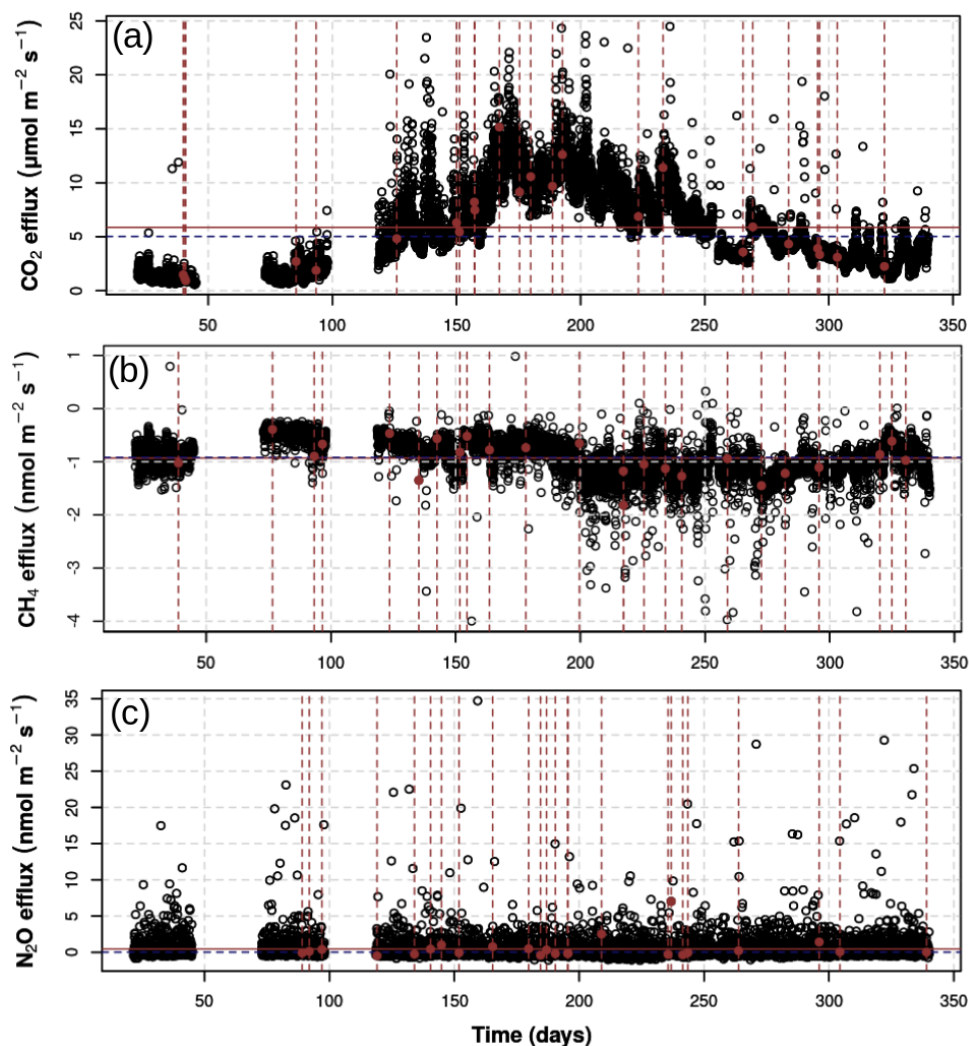


454
455
456
457

458 **Figure 1.** Temporal distribution of fixed temporal stratification (i.e., stratified manual
459 sampling approach) and optimized sampling using a temporal univariate Latin Hypercube
460 (*tuLHs*) approach for: $k=12$ (a), $k=24$ (b), and $k=48$ (c). Fixed temporal stratification is in
461 black, soil CO_2 fluxes in red, soil CH_4 fluxes in blue, and soil N_2O fluxes in green.



462

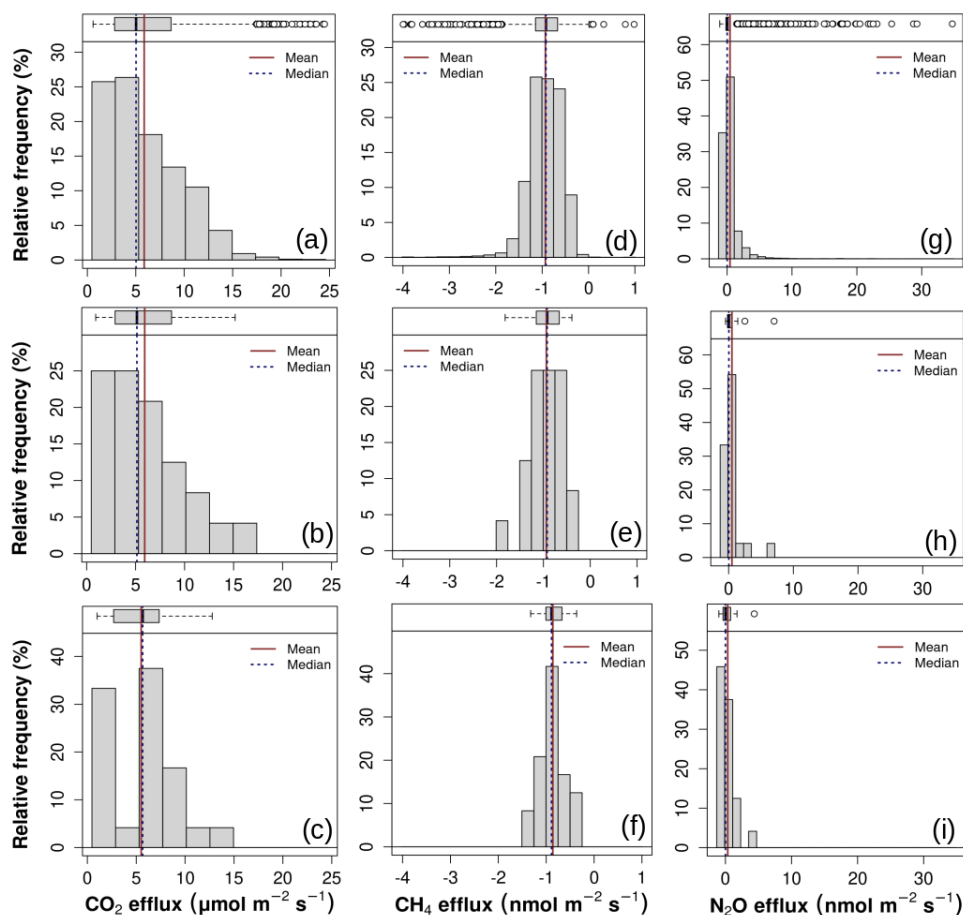


463
464
465
466
467
468
469
470
471
472

Figure 2. Time series of automated measurements (F_A) of soil greenhouse gas fluxes (black circles) and optimized samples ($k=24$) using a temporal univariate Latin Hypercube sampling (*tuLHs*) approach for soil CO_2 (a), soil CH_4 (b) and soil N_2O (c) fluxes. Horizontal red line represents the mean and horizontal blue line the median of each greenhouse gas flux derived from automated measurements. Selection of datapoints for $k=12$ and 48 are presented for each soil greenhouse gas time series in Figs. A3 and A4, respectively.

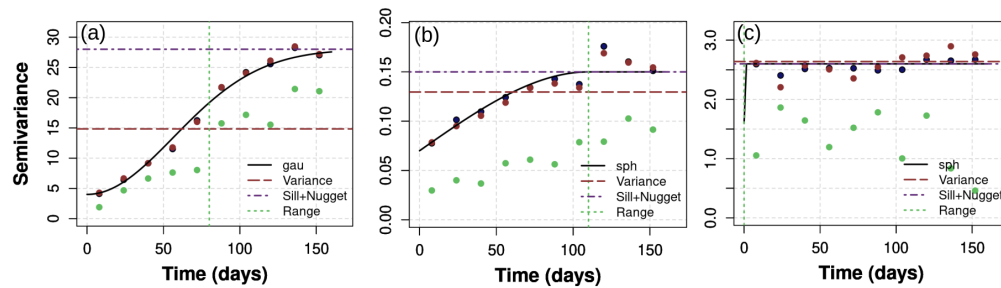


473



474
475
476
477
478
479
480
481
482
483
484

Figure 3. Histograms for automated measurements of soil CO₂ (F_A CO₂; a), soil CH₄ (F_A CH₄; d) and soil N₂O (F_A N₂O; g). Histograms for optimized samples ($k=24$) using a temporal univariate Latin Hypercube sampling (*tuLHs*) approach for soil CO₂ (b), soil CH₄ (e) and soil N₂O (h) fluxes. Histograms for fixed temporal stratification (i.e., stratified manual sampling schedule) ($k=24$) for soil CO₂ (c), soil CH₄ (f) and soil N₂O (i) fluxes. Appendix A includes results for measurements with $k=12$ (Fig. A5) and $k=48$ (Fig. A6).

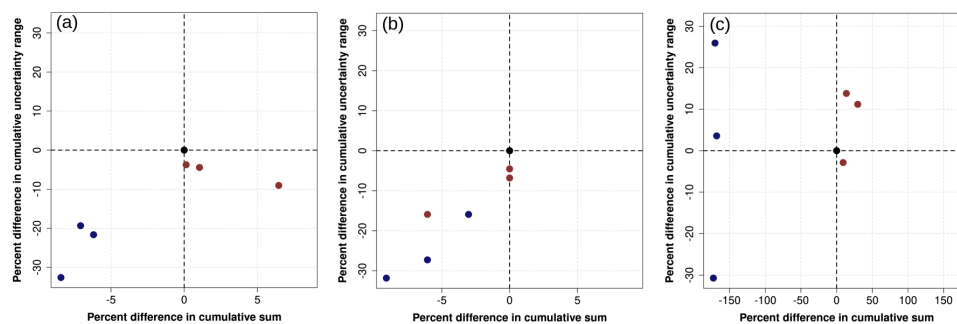


485
486
487
488
489
490
491
492
493
494
495
496
497

Figure 4. Comparison of semivariograms between automated measurements (F_A) of soil greenhouse gas fluxes (solid black line) and for optimized samples using a temporal univariate Latin Hypercube sampling (*tuLHs*) approach (red circles) or fixed temporal stratification (green circles) with $k=24$. Semivariograms are presented for soil CO_2 (a), CH_4 (d) and N_2O (c) fluxes. Semivariograms for measurements with $k=12$ and $k=48$ are presented in supplementary Figs. A7 and A8, respectively. Semivariogram fits were gaussian (Gau) or spherical (sph).



498



499
500
501
502
503
504
505
506
507
508
509
510
511
512
513
514
515

Figure 5. Comparison of percent differences from cumulative sums and associated uncertainty (95% CI) between greenhouse gas fluxes derived from automated measurements (F_A) and using an optimized sampling approach ($tuLHs$) or a fixed temporal stratification. Differences are represented for of soil CO₂ (a), soil CH₄ (b) and soil N₂O (c) fluxes. Black circle in the center (0,0) of a plot represents the values derived from automated measurements (F_A). Blue circles represent estimates from fixed temporal stratification, and red circles represent estimates from an optimized sampling approach ($tuLHs$). Estimates were calculated based on the 258 available automated measurements (Fig. 2) and numeric estimates are in Table A3.



516 **Appendix A – Supplementary Tables and Figures**

517

518 **Table A1.** Statistical properties for automated measurements of soil CO₂ (F_A CO₂), soil CH₄
 519 (F_A CH₄) and soil N₂O (F_A N₂O) fluxes, optimized samples ($k=12, 28, 48$) using a temporal
 520 univariate Latin Hypercube sampling (*tuLHs*), and fixed temporal stratification ($k=12, 28,$
 521 48). Units for soil CO₂ fluxes are in $\mu\text{mol m}^{-2} \text{s}^{-1}$, and for soil CH₄ and N₂O fluxes in nmol m^{-2}
 522 s^{-1} .

523

	Number of measurements (k)	1st. Quartile	Median	Mean	3rd. Quartile	Standard Deviation
$F_A\text{CO}_2$	8259	2.81	5.03	5.87	8.65	3.85
<i>tuLHs</i> approach (CO ₂)	12	3.19	5.30	6.25	8.88	4.06
	24	3.00	5.13	5.93	8.44	3.90
	48	2.84	4.97	5.88	8.54	3.87
Fixed temporal stratification (CO ₂)	12	2.68	5.82	5.37	7.10	3.15
	24	2.69	5.66	5.50	7.07	3.24
	48	2.69	5.53	5.45	8.05	3.29
$F_A\text{CH}_4$	8259	-1.14	-0.92	-0.93	-0.67	0.36
<i>tuLHs</i> approach (CH ₄)	12	-1.11	-0.89	-0.87	-0.66	0.33
	24	-1.14	-0.92	-0.94	-0.66	0.34
	48	-1.13	-0.91	-0.92	-0.66	0.35
Fixed temporal stratification (CH ₄)	12	-1.01	-0.83	-0.83	-0.67	0.27
	24	-1.01	-0.89	-0.86	-0.68	0.26
	48	-1.10	-0.86	-0.88	-0.66	0.29
$F_A\text{N}_2\text{O}$	8259	-0.18	0.01	0.45	0.49	1.62
<i>tuLHs</i> approach (N ₂ O)	12	-0.18	-0.01	0.58	0.50	1.58
	24	-0.18	0.03	0.51	0.45	1.54
	48	-0.17	0.02	0.49	0.45	1.54
Fixed temporal stratification (N ₂ O)	12	-0.35	0.51	0.59	0.83	1.38
	24	-0.21	-0.08	0.61	0.36	1.97
	48	-0.31	0.00	0.25	0.53	0.91

524



525 **Table A2.** Comparison of errors between experimental variogram for automated
 526 measurements of soil greenhouse gases (F_A ; $k=8259$) and experimental variograms for data
 527 using temporal univariate Latin Hypercube sampling (*tuLHs*) and fixed temporal
 528 stratification.
 529

	Approach	Number of measurements (k)	Error (Sum of absolute differences)
Soil CO ₂ fluxes	Fixed	12	69.31
		24	54.39
		48	49.42
	<i>tuLHs</i>	12	5.69
		24	1.99
		48	1.39
Soil CH ₄ fluxes	Fixed	12	0.63
		24	0.68
		48	0.49
	<i>tuLHs</i>	12	0.06
		24	0.04
		48	0.02
Soil N ₂ O fluxes	Fixed	12	10.01
		24	12.25
		48	16.75
	<i>tuLHs</i>	12	0.82
		24	1.13
		48	3.57

530
 531
 532
 533



534 **Table A3.** Cumulative sum and associated uncertainty of greenhouse gas (GHG) fluxes
 535 derived from automated measurements (F_A) and using an optimized sampling approach
 536 ($tuLHs$) or a fixed temporal stratification. Cumulative sum represents the total flux from
 537 available measurements derived from automated measurements for all GHG fluxes.
 538
 539

	Number of measurements (k)	Cumulative Sum	Uncertainty 95% CI		Uncertainty Range
F_{ACO_2} (g CO ₂ m ²)	8259	5758	893	13860	12966
$tuLHs$ approach (g CO ₂ m ²)	12	6130	1423	13218	11794
	24	5818	1046	13438	12391
	48	5766	946	13429	12482
Fixed temporal stratification (g CO ₂ m ²)	12	5273	1376	10117	8740
	24	5402	1196	11356	10160
	48	5351	1162	11621	10458
F_{ACH_4} (g CH ₄ m ²)	8259	-0.33	-0.58	-0.14	0.44
$tuLHs$ approach (g CH ₄ m ²)	12	-0.31	-0.49	-0.12	0.37
	24	-0.33	-0.57	-0.16	0.41
	48	-0.33	-0.56	-0.14	0.42
Fixed temporal stratification (g CH ₄ m ²)	12	-0.3	-0.45	-0.15	0.3
	24	-0.31	-0.46	-0.14	0.32
	48	-0.32	-0.51	-0.14	0.37
F_{AN_2O} (g N ₂ O m ²)	8259	0.44	-0.53	3.67	4.2
$tuLHs$ approach (g N ₂ O m ²)	12	0.57	-0.48	4.19	4.67
	24	0.5	-0.43	4.35	4.78
	48	0.48	-0.5	3.58	4.08
	12	-0.3	-0.83	3.52	4.35
	24	-0.31	-0.43	4.86	5.29



540

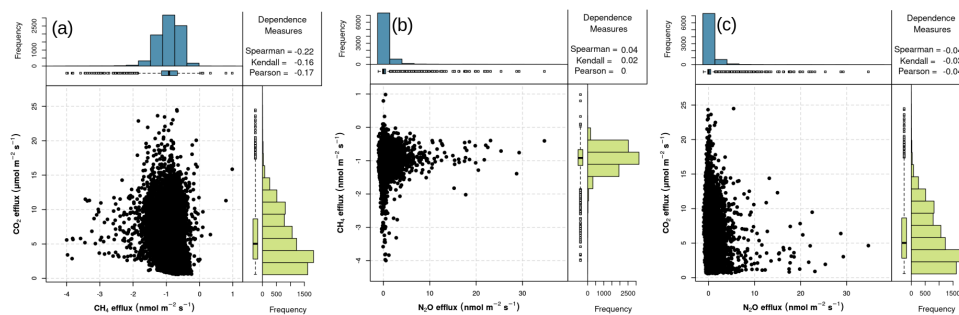
541

542

Fixed temporal stratification (g N ₂ O m ²)	48	-0.32	-0.7	2.21	2.91
---	----	-------	------	------	------



543
544
545

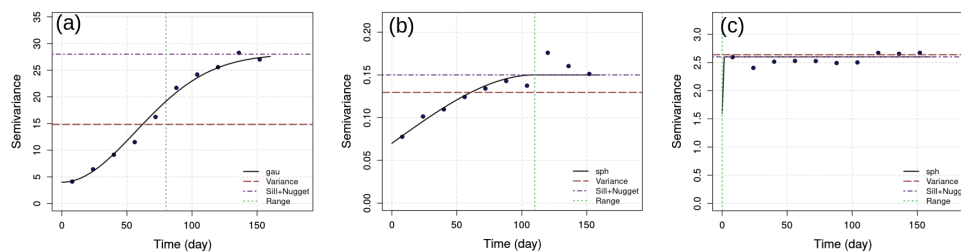


546
547
548
549
550
551
552
553

Figure A1. Relationships between soil CO₂ (F_A CO₂) with soil CH₄ (F_A CH₄) fluxes (a), soil CH₄ (F_A CH₄) with soil N₂O (F_A N₂O) fluxes (b), and soil CO₂ (F_A CO₂) with soil N₂O (F_A N₂O) fluxes. None of these relationships were significant at $\alpha=0.05$. These relationships were derived using all available data from automated measurements (F_A) of soil greenhouse gas fluxes.



554

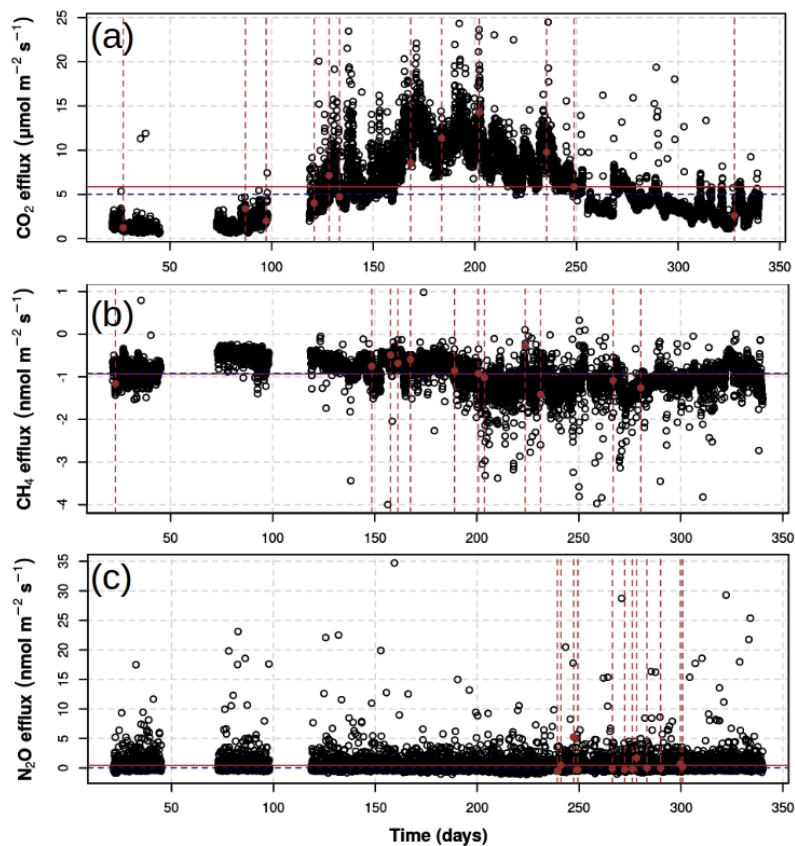


555
556

557 **Figure A2.** Semivariograms of soil CO₂ (F_A CO₂; a), soil CH₄ (F_A CH₄; b) and soil N₂O (F_A
558 N₂O; c) fluxes. These semivariograms were derived using all available data from automated
559 measurements (F_A) of soil greenhouse gas fluxes. Semivariogram fits were gaussian (Gau) or
560 spherical (sph).
561
562



563



564

565

566

567

568

569

570

571

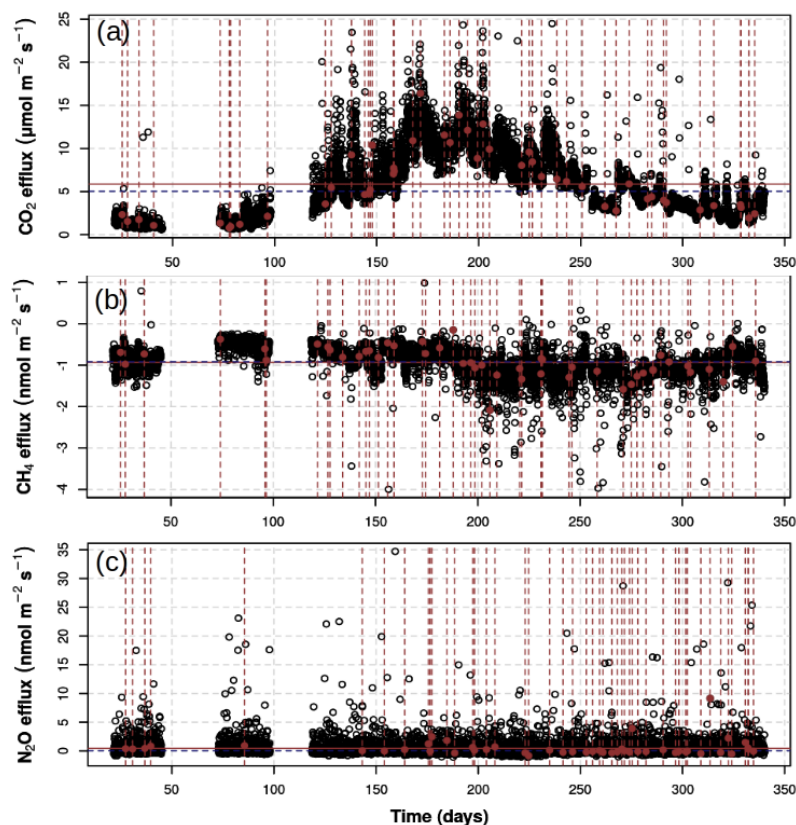
572

573

Figure A3. Time series of automated measurements (FA) of soil greenhouse gas fluxes (black circles) and optimized samples ($k=12$) using a temporal univariate Latin Hypercube sampling (*tuLHs*) approach for soil CO₂ (a), soil CH₄ (b) and soil N₂O (c) fluxes. Horizontal red line represents the mean and horizontal blue line the median of each greenhouse gas flux derived from automated measurements.

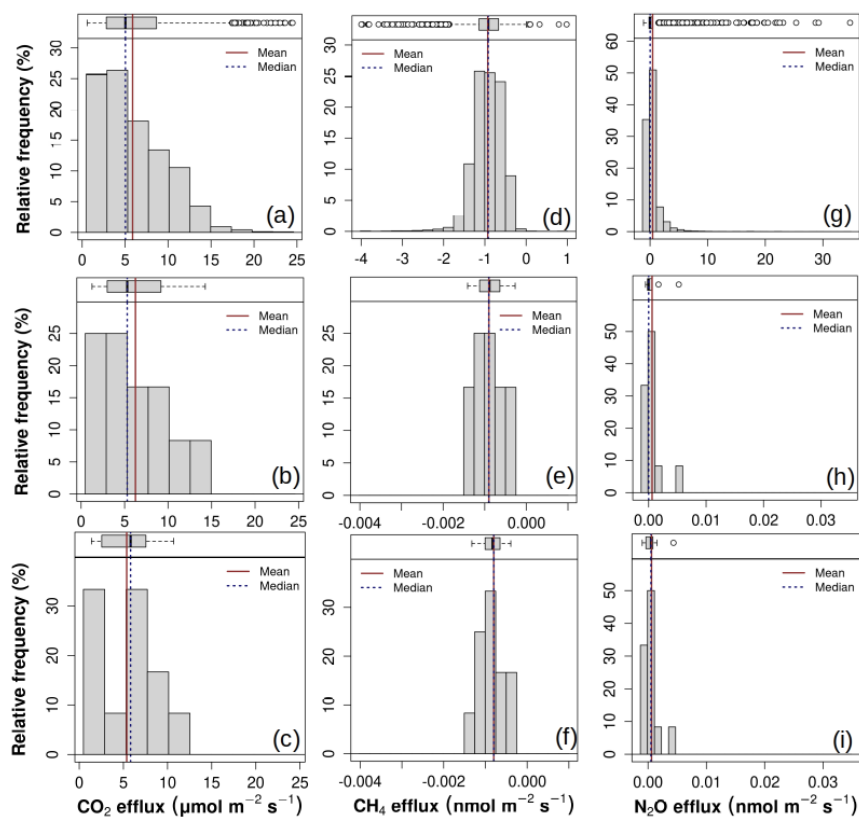


574
575
576
577
578



579
580
581
582
583
584
585
586
587
588
589
590
591
592
593
594

Figure A4. Time series of automated measurements (FA) of soil greenhouse gas fluxes (black circles) and optimized samples ($k=48$) using a temporal univariate Latin Hypercube sampling (*tuLHs*) approach for soil CO_2 (a), soil CH_4 (b) and soil N_2O (c) fluxes. Horizontal red line represents the mean and horizontal blue line the median of each greenhouse gas flux derived from automated measurements.

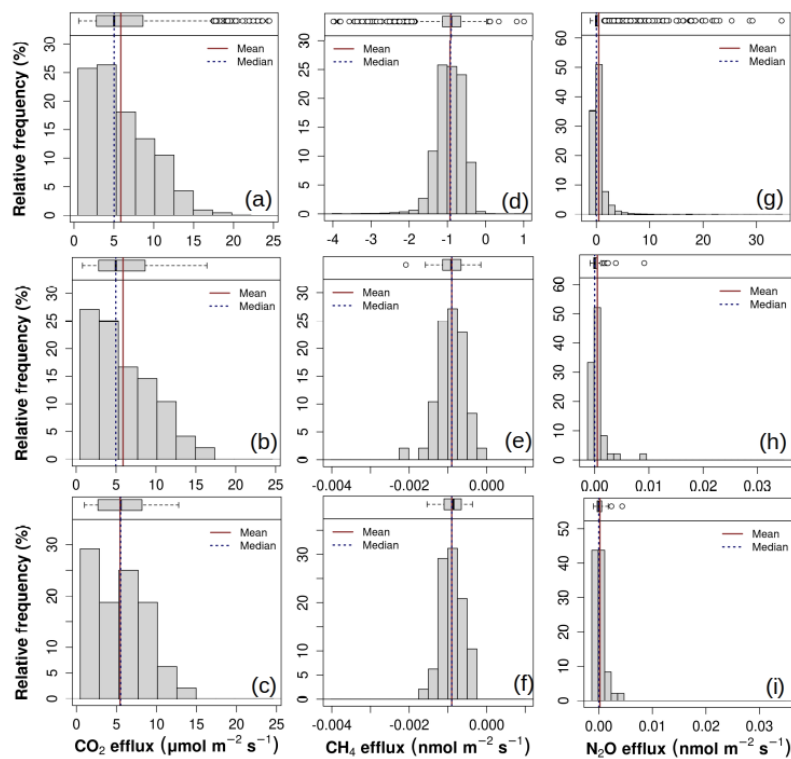


595
596
597
598
599
600
601
602
603
604

Figure A5. Histograms for automated measurements of soil CO₂ (F_A CO₂; a), soil CH₄ (F_A CH₄; d) and soil N₂O (F_A N₂O; g) fluxes. Histograms for optimized samples ($k=12$) using a temporal univariate Latin Hypercube sampling (*tuLHs*) approach for soil CO₂ (b), soil CH₄ (e) and soil N₂O (h) fluxes. Histograms for fixed temporal stratification (i.e., stratified manual sampling schedule; $k=12$) for soil CO₂ (c), soil CH₄ (f) and soil N₂O (i) fluxes.



605

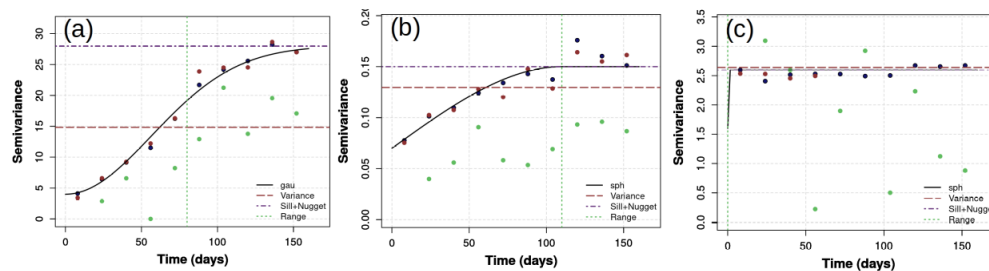


606
607
608
609
610
611
612
613
614

Figure A6. Histograms for automated measurements of soil CO₂ (F_A CO₂; a), soil CH₄ (F_A CH₄; d) and soil N₂O (F_A N₂O; g) fluxes. Histograms for optimized samples ($k=48$) using a temporal univariate Latin Hypercube sampling (*tuLHs*) approach for soil CO₂ (b), soil CH₄ (e) and soil N₂O (h) fluxes. Histograms for fixed temporal stratification (i.e., stratified manual sampling schedule; $k=48$) for soil CO₂ (c), soil CH₄ (f) and soil N₂O (i) fluxes.



615

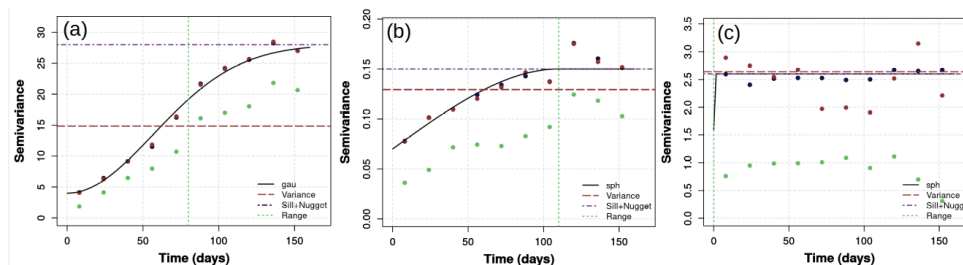


616
617
618
619
620
621
622
623
624
625
626
627

Figure A7. Comparison of semivariograms between automated measurements (F_A) of soil greenhouse gas fluxes (solid black line) and for optimized (red circles) or fixed temporal stratification (green circles) with $k=12$. Semivariograms are presented for soil CO_2 (a), CH_4 (d) and N_2O (c) fluxes. Semivariogram fits were gaussian (Gau) or spherical (sph).



628



629

630

631

632

633

634

635

636

637

Figure A8. Comparison of semivariograms between automated measurements (F_A) of soil greenhouse gas fluxes (solid black line) and for optimized (red circles) or fixed temporal stratification (green circles) with $k=48$. Semivariograms are presented for soil CO₂ (a), CH₄ (b) and N₂O (c) fluxes. Semivariogram fits were gaussian (Gau) or spherical (sph).



638 **References**

- 639 Anderegg, W. R. L.: Gambling With the Climate: How Risky of a Bet Are Natural Climate
640 Solutions?, <https://doi.org/10.1029/2021AV000490>, September 2021.
- 641 Bahn, M., Reichstein, M., Davidson, E. A., Gruenzweig, J., Jung, M., Carbone, M. S., Epron,
642 D., Misson, L., Nouvellon, Y., Roupsard, O., Savage, K., Trumbore, S. E., Gimeno, C.,
643 Curiel Yuste, J., Tang, J., Vargas, R., and Janssens, I. A.: Soil respiration at mean annual
644 temperature predicts annual total across vegetation types and biomes, *Biogeosciences*, 7,
645 2147–2157, 2010.
- 646 Ball, B. C.: Soil structure and greenhouse gas emissions: a synthesis of 20 years of
647 experimentation, *Eur. J. Soil Sci.*, 64, 357–373, 2013.
- 648 Barba, J., Poyatos, R., and Vargas, R.: Automated measurements of greenhouse gases fluxes
649 from tree stems and soils: magnitudes, patterns and drivers, *Sci. Rep.*, 9, 4005, 2019.
- 650 Barba, J., Poyatos, R., Capooci, M., and Vargas, R.: Spatiotemporal variability and origin of
651 CO₂ and CH₄ tree stem fluxes in an upland forest, *Glob. Chang. Biol.*, 27, 4879–4893, 2021.
- 652 Bond-Lamberty, B., Christianson, D. S., Malhotra, A., Pennington, S. C., Sili, D.,
653 AghaKouchak, A., Anjileli, H., Altaf Arain, M., Armesto, J. J., Ashraf, S., Ataka, M.,
654 Baldocchi, D., Andrew Black, T., Buchmann, N., Carbone, M. S., Chang, S., Crill, P., Curtis,
655 P. S., Davidson, E. A., Desai, A. R., Drake, J. E., El-Madany, T. S., Gavazzi, M., Görres, C.,
656 Gough, C. M., Goulden, M., Gregg, J., Gutiérrez del Arroyo, O., He, J., Hirano, T., Hopple,
657 A., Hughes, H., Järveoja, J., Jassal, R., Jian, J., Kan, H., Kaye, J., Kominami, Y., Liang, N.,
658 Lipson, D., Macdonald, C. A., Maseyk, K., Mathes, K., Mauritz, M., Mayes, M. A.,
659 McNulty, S., Miao, G., Migliavacca, M., Miller, S., Miniati, C. F., Nietz, J. G., Nilsson, M.
660 B., Noormets, A., Norouzi, H., O’Connell, C. S., Osborne, B., Oyonarte, C., Pang, Z., Peichl,



- 661 M., Pendall, E., Perez-Quezada, J. F., Phillips, C. L., Phillips, R. P., Raich, J. W., Renchon,
662 A. A., Ruehr, N. K., Sánchez-Cañete, E. P., Saunders, M., Savage, K. E., Schrumpf, M.,
663 Scott, R. L., Seibt, U., Silver, W. L., Sun, W., Szutu, D., Takagi, K., Takagi, M., Teramoto,
664 M., Tjoelker, M. G., Trumbore, S., Ueyama, M., Vargas, R., Varner, R. K., Verfaillie, J.,
665 Vogel, C., Wang, J., Winston, G., Wood, T. E., Wu, J., Wutzler, T., Zeng, J., Zha, T., Zhang,
666 Q., and Zou, J.: COSORE: A community database for continuous soil respiration and other
667 soil-atmosphere greenhouse gas flux data, *Glob. Chang. Biol.*, 249, 434, 2020.
- 668 Bossio, D. A., Cook-Patton, S. C., Ellis, P. W., Fargione, J., Sanderman, J., Smith, P., Wood,
669 S., Zomer, R. J., von Unger, M., Emmer, I. M., and Griscom, B. W.: The role of soil carbon
670 in natural climate solutions, *Nature Sustainability*, 3, 391–398, 2020.
- 671 Bouma, J.: Chapter 4 - Implications of the Knowledge Paradox for Soil Science, in:
672 *Advances in Agronomy*, vol. 106, edited by: Sparks, D. L., Academic Press, 143–171, 2010.
- 673 Bowden, R. D., Castro, M. S., Melillo, J. M., Steudler, P. A., and Aber, J. D.: Fluxes of
674 greenhouse gases between soils and the atmosphere in a temperate forest following a
675 simulated hurricane blowdown, *Biogeochemistry*, 21, 61–71, 1993.
- 676 Bowden, R. D., Newkirk, K. M., and Rullo, G. M.: Carbon dioxide and methane fluxes by a
677 forest soil under laboratory-controlled moisture and temperature conditions, *Soil Biol.*
678 *Biochem.*, 30, 1591–1597, 1998.
- 679 Bréchet, L. M., Daniel, W., Stahl, C., Burban, B., Goret, J.-Y., Salomón, R. L., and Janssens,
680 I. A.: Simultaneous tree stem and soil greenhouse gas (CO₂, CH₄, N₂O) flux
681 measurements: a novel design for continuous monitoring towards improving flux estimates
682 and temporal resolution, *New Phytol.*, 230, 2487–2500, 2021.



- 683 Butterbach-Bahl, K., Kock, M., Willibald, G., Hewett, B., Buhagiar, S., Papen, H., and Kiese,
684 R.: Temporal variations of fluxes of NO, NO₂, N₂O, CO₂, and CH₄ in a tropical rain forest
685 ecosystem, *Global Biogeochem. Cycles*, 18, <https://doi.org/10.1029/2004gb002243>, 2004.
- 686 Capooci, M. and Vargas, R.: Diel and seasonal patterns of soil CO₂ efflux in a temperate
687 tidal marsh, *Sci. Total Environ.*, 802, 149715, 2022.
- 688 Capooci, M., Barba, J., Seyfferth, A. L., and Vargas, R.: Experimental influence of storm-
689 surge salinity on soil greenhouse gas emissions from a tidal salt marsh, *Sci. Total Environ.*,
690 686, 1164–1172, 2019.
- 691 Castro, M. S., Melillo, J. M., Steudler, P. A., and Chapman, J. W.: Soil moisture as a
692 predictor of methane uptake by temperate forest soils, *Can. J. For. Res.*, 24, 1805–1810,
693 1994.
- 694 Castro, M. S., Steudler, P. A., Melillo, J. M., Aber, J. D., and Bowden, R. D.: Factors
695 controlling atmospheric methane consumption by temperate forest soils, *Global Biogeochem.*
696 *Cycles*, 9, 1–10, 1995.
- 697 Chilès, J.-P. and Delfiner, P.: *Geostatistics: Modeling Spatial Uncertainty*, John Wiley &
698 Sons, 720 pp., 2009.
- 699 Cueva, A., Bullock, S. H., López-Reyes, E., and Vargas, R.: Potential bias of daily soil CO₂
700 efflux estimates due to sampling time, *Sci. Rep.*, 7, 11925, 2017.
- 701 Freeman, C., Lock, M. A., and Reynolds, B.: Fluxes of CO₂, CH₄ and N₂O from a Welsh
702 peatland following simulation of water table draw-down: Potential feedback to climatic
703 change, *Biogeochemistry*, 19, <https://doi.org/10.1007/bf00000574>, 1993.



- 704 Griscom, B. W., Adams, J., Ellis, P. W., Houghton, R. A., Lomax, G., Miteva, D. A.,
705 Schlesinger, W. H., Shoch, D., Siikamäki, J. V., Smith, P., Woodbury, P., Zganjar, C.,
706 Blackman, A., Campari, J., Conant, R. T., Delgado, C., Elias, P., Gopalakrishna, T., Hamsik,
707 M. R., Herrero, M., Kiesecker, J., Landis, E., Laestadius, L., Leavitt, S. M., Minnemeyer, S.,
708 Polasky, S., Potapov, P., Putz, F. E., Sanderman, J., Silvius, M., Wollenberg, E., and
709 Fargione, J.: Natural climate solutions, *Proc. Natl. Acad. Sci. U. S. A.*, 114, 11645–11650,
710 2017.
- 711 Gunawardana, A., Meek, C., and Xu, P.: A model for temporal dependencies in event
712 streams, *Adv. Neural Inf. Process. Syst.*, 24, 2011.
- 713 Hao, W. M., Scharffe, D., Crutzen, P. J., and Sanhueza, E.: Production of N₂O, CH₄, and
714 CO₂ from soils in the tropical savanna during the dry season, *J. Atmos. Chem.*, 7, 93–105,
715 1988.
- 716 Hill, A. C., Barba, J., Hom, J., and Vargas, R.: Patterns and drivers of multi-annual CO₂
717 emissions within a temperate suburban neighborhood, *Biogeochemistry*, 152, 35–50, 2021.
- 718 Huntington, D. E. and Lyrintzis, C. S.: Improvements to and limitations of Latin hypercube
719 sampling, *Probab. Eng. Mech.*, 13, 245–253, 1998.
- 720 Hutchinson, G. E.: The Concept of Pattern in Ecology, 105, 1–12, 1953.
- 721 Jian, J., Vargas, R., Anderson-Teixeira, K., Stell, E., Herrmann, V., Horn, M., Kholod, N.,
722 Manzon, J., Marchesi, R., Paredes, D., and Bond-Lamberty, B.: A restructured and updated
723 global soil respiration database (SRDB-V5), *Data, Algorithms, and Models*,
724 <https://doi.org/10.5194/essd-2020-136>, 2020.



- 725 Keller, M., Kaplan, W. A., and Wofsy, S. C.: Emissions of N₂O, CH₄ and CO₂ from tropical
726 forest soils, *J. Geophys. Res.*, 91, 11791, 1986.
- 727 Kim, D. G., Vargas, R., Bond-Lamberty, B., and Turetsky, M. R.: Effects of soil rewetting
728 and thawing on soil gas fluxes: a review of current literature and suggestions for future
729 research, *Biogeosciences*, 9, 2459–2483, 2012.
- 730 Le, V. H., Díaz-Viera, M. A., Vázquez-Ramírez, D., del Valle-García, R., Erdely, A., and
731 Grana, D.: Bernstein copula-based spatial cosimulation for petrophysical property prediction
732 conditioned to elastic attributes, *J. Pet. Sci. Eng.*, 193, 107382, 2020.
- 733 Lucas-Moffat, A. M., Huth, V., Augustin, J., Brümmer, C., Herbst, M., and Kutsch, W. L.:
734 Towards pairing plot and field scale measurements in managed ecosystems: Using eddy
735 covariance to cross-validate CO₂ fluxes modeled from manual chamber campaigns, *Agric.*
736 *For. Meteorol.*, 256–257, 362–378, 2018.
- 737 Luo, G. J., Kiese, R., Wolf, B., and Butterbach-Bahl, K.: Effects of soil temperature and
738 moisture on methane uptake and nitrous oxide emissions across three different ecosystem
739 types, *Biogeosciences*, 10, 3205–3219, 2013.
- 740 Oertel, C., Matschullat, J., Zurba, K., Zimmermann, F., and Erasmi, S.: Greenhouse gas
741 emissions from soils—A review, *Geochem. Explor. Environ. Analy.*, 76, 327–352, 2016.
- 742 Ojanen, P., Minkkinen, K., Alm, J., and Penttilä, T.: Soil–atmosphere CO₂, CH₄ and N₂O
743 fluxes in boreal forestry-drained peatlands, *For. Ecol. Manage.*, 260, 411–421, 2010.
- 744 Petrakis, S., Seyfferth, A., Kan, J., Inamdar, S., and Vargas, R.: Influence of experimental
745 extreme water pulses on greenhouse gas emissions from soils, *Biogeochemistry*, 133, 147–
746 164, 2017.



- 747 Petrakis, S., Barba, J., Bond-Lamberty, B., and Vargas, R.: Using greenhouse gas fluxes to
748 define soil functional types, *Plant Soil*, 423, 285–294, 2018.
- 749 Phillips, C. L., Bond-Lamberty, B., Desai, A. R., Lavoie, M., Risk, D., Tang, J. W., Todd-
750 Brown, K., and Vargas, R.: The value of soil respiration measurements for interpreting and
751 modeling terrestrial carbon cycling, *Plant Soil*, 413, 1–25, 2017.
- 752 Pyrcz, M. J. and Deutsch, C. V.: *Geostatistical Reservoir Modeling*, OUP USA, 433 pp.,
753 2014.
- 754 Rowlings, D. W., Grace, P. R., Kiese, R., and Weier, K. L.: Environmental factors
755 controlling temporal and spatial variability in the soil-atmosphere exchange of CO₂, CH₄
756 and N₂O from an Australian subtropical rainforest, *Glob. Chang. Biol.*, 18, 726–738, 2012.
- 757 Savage, K., Phillips, R., and Davidson, E.: High temporal frequency measurements of
758 greenhouse gas emissions from soils, *Biogeosciences*, 11, 2709–2720, 2014.
- 759 Shakoor, A., Shahbaz, M., Farooq, T. H., Sahar, N. E., Shahzad, S. M., Altaf, M. M., and
760 Ashraf, M.: A global meta-analysis of greenhouse gases emission and crop yield under no-
761 tillage as compared to conventional tillage, *Sci. Total Environ.*, 750, 142299, 2021.
- 762 Storn, R. and Price, K.: Differential Evolution – A Simple and Efficient Heuristic for global
763 Optimization over Continuous Spaces, *J. Global Optimiz.*, 11, 341–359, 1997.
- 764 Tallec, T., Brut, A., Joly, L., Dumelié, N., Serça, D., Mordelet, P., Claverie, N., Legain, D.,
765 Barrié, J., Decarpenterie, T., Cousin, J., Zawilski, B., Ceschia, E., Guérin, F., and Le Dantec,
766 V.: N₂O flux measurements over an irrigated maize crop: A comparison of three methods,
767 *Agric. For. Meteorol.*, 264, 56–72, 2019.



- 768 Tang, X., Liu, S., Zhou, G., Zhang, D., and Zhou, C.: Soil-atmospheric exchange of CO₂ ,
769 CH₄ , and N₂ O in three subtropical forest ecosystems in southern China, *Glob. Chang. Biol.*,
770 12, 546–560, 2006.
- 771 Trangmar, B. B., Yost, R. S., and Uehara, G.: Application of Geostatistics to Spatial Studies
772 of Soil Properties, in: *Advances in Agronomy*, vol. 38, edited by: Brady, N. C., Academic
773 Press, 45–94, 1986.
- 774 Ullah, S. and Moore, T. R.: Biogeochemical controls on methane, nitrous oxide, and carbon
775 dioxide fluxes from deciduous forest soils in eastern Canada, *J. Geophys. Res.*, 116,
776 <https://doi.org/10.1029/2010jg001525>, 2011.
- 777 Vargas, R.: How a hurricane disturbance influences extreme CO₂ fluxes and variance in a
778 tropical forest, *Environ. Res. Lett.*, 2012.
- 779 Vargas, R., Carbone, M. S., Reichstein, M., and Baldocchi, D. D.: Frontiers and challenges in
780 soil respiration research: from measurements to model-data integration, *Biogeochemistry*,
781 102, 1–13, 2011.
- 782 Vargas, R., Sánchez-Cañete P., E., Serrano-Ortiz, P., Curiel Yuste, J., Domingo, F., López-
783 Ballesteros, A., and Oyonarte, C.: Hot-Moments of Soil CO₂ Efflux in a Water-Limited
784 Grassland, *Soil Systems*, 2, 47, 2018.
- 785 Vicca, S., Bahn, M., Estiarte, M., van Loon, E. E., Vargas, R., Alberti, G., Ambus, P., Arain,
786 M. A., Beier, C., Bentley, L. P., Borken, W., Buchmann, N., Collins, S. L., de Dato, G.,
787 Dukes, J. S., Escolar, C., Fay, P., Guidolotti, G., Hanson, P. J., Kahmen, A., Kröel-Dulay, G.,
788 Ladreiter-Knauss, T., Larsen, K. S., Lellei-Kovacs, E., Lebrija-Trejos, E., Maestre, F. T.,
789 Marhan, S., Marshall, M., Meir, P., Miao, Y., Muhr, J., Niklaus, P. A., Ogaya, R., Peñuelas,



- 790 J., Poll, C., Rustad, L. E., Savage, K., Schindlbacher, A., Schmidt, I. K., Smith, A. R., Sotta,
791 E. D., Suseela, V., Tietema, A., van Gestel, N., van Straaten, O., Wan, S., Weber, U., and
792 Janssens, I. A.: Can current moisture responses predict soil CO₂ efflux under altered
793 precipitation regimes? A synthesis of manipulation experiments, *Biogeosciences*, 11, 2991–
794 3013, 2014.
- 795 Villarreal, S., Guevara, M., Alcaraz-Segura, D., and Vargas, R.: Optimizing an
796 Environmental Observatory Network Design Using Publicly Available Data, *J. Geophys.*
797 *Res. Biogeosci.*, 124, 1812–1826, 2019.
- 798 Wang, G. and Chen, S.: A review on parameterization and uncertainty in modeling
799 greenhouse gas emissions from soil, *Geoderma*, 170, 206–216, 2012.
- 800 Werner, C., Kiese, R., and Butterbach-Bahl, K.: Soil-atmosphere exchange of N₂O, CH₄,
801 and CO₂ and controlling environmental factors for tropical rain forest sites in western Kenya,
802 *J. Geophys. Res.*, 112, <https://doi.org/10.1029/2006jd007388>, 2007.
- 803 Wu, X., Brüggemann, N., Gasche, R., Shen, Z., Wolf, B., and Butterbach-Bahl, K.:
804 Environmental controls over soil-atmosphere exchange of N₂O, NO, and CO₂ in a temperate
805 Norway spruce forest, *Global Biogeochem. Cycles*, 24,
806 <https://doi.org/10.1029/2009gb003616>, 2010.
- 807 Yao, Z., Zheng, X., Xie, B., Liu, C., Mei, B., Dong, H., Butterbach-Bahl, K., and Zhu, J.:
808 Comparison of manual and automated chambers for field measurements of N₂O, CH₄, CO₂
809 fluxes from cultivated land, *Atmos. Environ.*, 43, 1888–1896, 2009.